Dew deposition suppresses transpiration and carbon uptake in leaves

Cynthia Gerlein-Safdi[a,*], Michael C. Koohafkan[b,c], Michaella Chung[c], Fulton E. Rockwell[d], Sally Thompson[c], Kelly K. Caylor[a,e,f]

[a] Department of Civil and Environmental Engineering, Princeton University, Princeton, NJ 08544, USA
[b] Hydrologic Sciences Graduate Group, University of California Davis, Davis, CA 95616, USA
[c] Department of Civil and Environmental Engineering, University of California Berkeley, Berkeley, CA 94720, USA
[d] Department of Organismic and Evolutionary Biology, Harvard University, Cambridge, MA 02138, USA
[e] Department of Geography, University of California Santa Barbara, Santa Barbara, CA 93106, USA
[f] Bren School of Environmental Science and Management, UC Santa Barbara, Santa Barbara, CA 93106, USA

ABSTRACT

Dew deposition occurs in ecosystems worldwide, even in the driest deserts and in times of drought. Although some species absorb dew water directly via foliar uptake, a ubiquitous effect of dew on plant water balance is the interference of dew droplets with the leaf energy balance, which increases leaf albedo and emissivity and decreases leaf temperature through dew evaporation. Dew deposition frequency and amount are expected to be affected by changing environmental conditions, with unknown consequences for plant water stress and ecosystem carbon, water and energy fluxes. Here we present a simple leaf energy balance that characterizes the effect of deposition and the evaporation of dew on leaf energy balance, transpiration, and carbon uptake. The model is driven by five common meteorological variables and shows very good agreement with leaf wetness sensor data from the Blue Oak Ranch Reserve in California. We explore the tradeoffs between energy, water, and carbon balances for leaves of different sizes across a range of relative humidity, wind speed, and air temperature conditions. Our results show significant water savings from transpiration suppression up to 25% for leaf characteristic lengths of 50 cm. CO_2 assimilation is decreased by up to 12% by the presence of dew, except for bigger leaves in windspeed conditions below $1 \, \text{m} \, \text{s}^{-1}$ when an increase in assimilation is expected.

1. Introduction

Non-meteoric water (dew or fog) is an often-overlooked component of surface water balance for many landscapes. Dew in particular can occur in virtually every climate and ecosystem worldwide, from the arid Negev Desert of Israel (Zangvil, 1996; Hill et al., 2015), to flooded rice paddies of China (Xu et al., 2015), semi-arid costal steppes of Spain (Uclés et al., 2013), American wheat fields (Pinter, 1986), lush Northern European lawns (Monteith, 1957; Jacobs et al., 2006), and tropical forests (Clus et al., 2008; Lakatos et al., 2012). Non-meteoric water can affect the water balance of plants directly through foliar uptake (Yates and Hutley, 1995; Andrade, 2003; Lakatos et al., 2012; Berkelhammer et al., 2013), and can act as a major water source for vegetation where fresh water is scarce (Agam and Berliner, 2006; Clus et al., 2008). Some species that lack access to soil water – including epiphytic bromeliads (Andrade, 2003; Gotsch et al., 2015; Pan and Wang, 2014) and lichens (Lakatos et al., 2012) – have physical features allowing them to collect dew water. Most plant species, however, have

water-repellent leaves (Neinhuis and Barthlott, 1997) that are adapted to shed water rather than trapping and imbibing it. Non-meteoric water deposition can impose risk on plants: in cold climates it may freeze, damaging leaf tissue (Jordan and Smith, 1994), and in warm environments it may cause rotting and facilitate pathogen infection (Evans et al., 1992). As a response, many species have developed waxy, hydrophobic cuticles (Holloway, 1994) that force water droplets to bead up and roll off the leaf. However, the capacity for droplets to drain off the leaf can be very small (Gao and McCarthy, 2006), in spite of high contact angles between droplet and leaf surface (Holder, 2012b). Therefore, during dew events, micro-droplets of water may sometimes form on the surface of even hydrophobic leaves (Holder, 2012b; Aparecido et al., 2017).

The accumulation of dew droplets on leaf surfaces directly affects leaf energy balance through evaporative cooling, changes in albedo, and changes in emissivity. These factors – and their interactions – lead to transpiration suppression – a collective term that describes reductions in leaf-level transpiration (Tolk et al., 1995; Gerlein-Safdi et al.,

2018). There is growing interest in transpiration suppression during interactions between leaves and non-meteoric water (Barradas and Glez-Medellín, 1999; Alvarado-Barrientos et al., 2014), but the importance of transpiration suppression to leaf water status and the specific manner by which dew deposition affects leaf energy, water, and carbon balances and the magnitude of these effects are still poorly resolved.

The leaf energy balance is often considered at steady state, a condition when energy inputs due to net shortwave radiation, K (W m^{-2}), and incoming longwave radiation, L_{in} (W m^{-2}), are balanced by the energy losses due to outgoing longwave radiation, L_{out} (W m^{-2}), sensible heat transfers due to convection, H (W m^{-2}), and latent energy transfers associated with the exothermic evaporation of liquid water within the leaf, λE (W m^{-2}), where λ is the latent heat of vaporization of water (J kg^{-1}) (Gates, 1980; Vogel, 2012). The steady state energy balance can be expressed as (Campbell and Norman, 1998):

$$K + L_{in} = \lambda E + H + L_{out} \qquad (1)$$

which can be simplified to:

$$R_n = \lambda E + H, \qquad (2)$$

where $R_n = K + L_{in} - L_{out}$ is the net radiation (W m^{-2}). Because the leaf energy loss processes are temperature-dependent, a steady state energy balance implies a steady state leaf temperature. In natural ecosystems, this leaf temperature is generally warmer than surrounding air, due to the high radiative fluxes leaves experience, and their low thermal mass (Li et al., 2013). Smaller leaves tend to be at a temperature closer to the ambient air, because their boundary layer is thinner, facilitating convective heat exchange (Givnish, 1987; Scoffoni et al., 2011). For this reason, and because high leaf temperatures can impede photosynthesis or even result in leaf mortality, sun-exposed leaves are often smaller than shaded leaves (Gates, 1980).

The λE term in Eq. (1) couples steady-state leaf energy balance to steady-state plant water balance, because evaporating water in leaves must be replaced by transport of water to the leaf via the xylem. Indeed, plants open their stomata to allow CO_2 to diffuse in, with an inevitable loss of water as water vapor diffuses out. This water loss leads to evaporative cooling, which plays an important role in balancing solar radiative forcing (Pieruschka et al., 2010). When plant available water is insufficient to meet lead water demand under ambient environmental conditions, leaf transpiration rates are reduced through stomatal closure, which leads to a new steady-state energy balance with a higher leaf temperature. Thus, drought conditions, which restrict leaf water supply, elevate leaf temperature, causing a trade-off between water conservation and temperature management (Rodriguez-Dominguez et al., 2016). Non-meteoric water on a leaf surface, however, increases - and externalizes – the water supply available for evaporative cooling (Chu et al., 2012), potentially alleviating this tradeoff. In the presence of non-meteoric leaf water, the leaf energy balance equation is modified:

$$R_n = \lambda E + H + E_{dew}, \qquad (3)$$

and evaporation of the dew (E_{dew}) provides an additional leaf energy sink. Applying this estimate to typical dew deposition volumes (0.5 mm/day (Monteith, 1963; Clus et al., 2008), with peak values of 0.8 mm/day reported in some tropical forests (Andrade, 2003; Lakatos et al., 2012)) suggests that dew evaporation could satiate $\approx 1/6$ of potential transpiration in tropical areas, less in arid climates (Monteith, 1963). These estimates, however, neglect two additional impacts of dew deposition on leaves: (1) wet leaves have higher albedos, which reduces K (Pinter, 1986); and (2) wet leave have a lower temperature, because of the cooling provided by dew evaporation which lowers fluxes of water (λE, E_{dew}) and energy (H) from the leaf. Because dew formed before dawn can persist for up to 6 h after sunrise (Abtew and Melesse, 2012; Monteith, 1957) and dew may also form in the late afternoon before sunset (Wilson et al., 1999; Kabela et al., 2009),

albedo and evaporative cooling effects can last for a considerable portion of the day (Aparecido et al., 2017), shortening the duration of water stress experienced by plants.

Dew deposition events are spatially extensive, and may occur simultaneously over areas of thousands of squared kilometers (de Jeu et al., 2005). Even small changes in leaf energy, water, and carbon balances on such scales can imply large landscape-scale impacts. The ubiquity of dew events across ecosystems and climates, including during drought events, points to potentially important implications of transpiration suppression from dew for drought survival (Yang et al., 2017) and plant community composition (Gauslaa, 2014; McLaughlin et al., 2017). Indeed, transpiration suppression by dew can help plants maintain healthy leaf water status during soil droughts (Madeira et al., 2002; Proctor, 2012). Key drivers of dew deposition, however, especially air temperature and relative humidity, are expected to change rapidly with climate change (Cook et al., 2014), especially in tropical forests (Malhi and Wright, 2004; Nepstad et al., 2008), and will likely cause changes in the frequency and amount of dew deposition (Vuollekoski et al., 2015; Tomaszkiewicz et al., 2016). For example, reduced dew formation was a key feature of the 2005 mega-drought in the Amazon (Frolking et al., 2011). Non-climate drivers of global change such as deforestation also impact dew and fog formation by raising temperatures and lowering humidity (Moreira et al., 1997; Ray et al., 2006). The ecological impact of such changes in dew formation regimes is unclear. Although dew formation is included in many global climate models (Rosenzweig and Abramopoulos, 1997), its interaction with vegetation carbon, energy, and water balance is not usually evaluated, which represents a missing climate-ecosystem feedback in evaluations of global change. However, including the interaction of vegetation with non-meteoric water in global climate models requires the development and testing of biophysical models of dew deposition, dew evaporation, and the consequences for leaf level carbon, energy and water balance.

Some important components of such a model have been developed in different contexts: (i) informing the design of dew collection systems to supplement water supply; and (ii) modeling effects of dew on agricultural disease risks. Independently, these efforts have provided detailed energy balance descriptions of synthetic condenser systems (Nikolayev et al., 1996; Jacobs et al., 2002; Richards, 2009; Maestre-Valero et al., 2012; Beysens, 2016) and the duration of leaf wetness on plant leaves (Janssen and Römer, 1991; Evans et al., 1992; Sentelhas et al., 2008; Schmitz and Grant, 2009; Bregaglio et al., 2010; Kim et al., 2010). The aim of this study is to link insight from these models to each other in order to develop a representation of the leaf carbon, energy, and water balance that provides a framework for interrogating the leaf-level physiological implications of dew deposition. To this end, we propose a new leaf energy balance model that incorporates both the deposition and the evaporation of dew. The energy balance model is coupled to a dynamic stomatal conductance and leaf carbon assimilation model that tracks the effect of the presence of dew on leaf temperature, transpiration, and CO_2 uptake. To test the model, we firstly present the results of a calibration experiment that relates the voltage reading on commercially available capacitance leaf wetness sensors to the mass of water accumulated on the surfaces of plant leaves exposed to the same conditions of humidity and temperature. The resulting calibration relationship is then used to infer the mass of dew stored on a network of similar leaf wetness sensors deployed across a range of elevation, vegetation, and topographic settings at Blue Oak Ranch Reserve, near San Jose California. Web camera images are used to identify a set of dew and low-density fog events, and leaf wetness sensor output is used to test model predictions based on locally observed temperature and humidity during these events. The model is then applied to quantify transpiration suppression and changes in CO_2 assimilation rates from dew deposition.

2. Materials and methods

2.1. Modeling the effects of dew on a leaf

2.1.1. Energy balance

Here, we present a process-based model of dew deposition on the adaxial surface of the leaf and dew evaporation, and its effect on leaf temperature, transpiration, and CO_2 uptake by coupling the heat equation to a dew mass balance equation (Richards, 2009; Vuollekoski et al., 2015). The heat equation describes the energy balance in terms of its effects on plant leaf temperature, as follows:

$$\frac{d\ T_{leaf}}{dt}\ (C_l\ m_l\ +\ C_d\ m_d)\ =\ S_l\ R_n\ +\ P_{lat}\ -\ S_l\ H\ -\ S_l\ \lambda E, \tag{4}$$

where T_{leaf}, C_l, and m_l are the leaf temperature in °C, leaf specific heat capacity in $J\,kg^{-1}\,K^{-1}$, and leaf mass in kg, respectively. C_d, and m_d are the specific heat capacity and mass of dew accumulated on the leaf. S_l is the surface area of the leaf in m^2, and R_n, H, and λE are in $W\,m^{-2}$, and P_{lat} is E_{dew} (Eq. (3)) expressed in W.

The net radiation R_n is described as:

$$R_n = \begin{cases} (1 - \alpha_{dew})\ R_{sw}\ +\ (\epsilon_w\ \epsilon_{atm} & \text{if } m_d > 0 \\ \quad +\ \epsilon_l\ \epsilon_{surr})\ \sigma\ (T_{air} + 273.2)^4\ -\ (\epsilon_l \\ \quad +\ \epsilon_w)\ \sigma\ (T_{leaf} + 273.2)^4, \\ (1 - \alpha_{dry})\ R_{sw}\ +\ \epsilon_l\ (\epsilon_{atm} & \text{if } m_d = 0 \\ \quad +\ \epsilon_{surr})\ \sigma\ (T_{air} + 273.2)^4 \\ \quad -\ 2\ \epsilon_l\ \sigma\ (T_{leaf} + 273.2)^4, \end{cases} \tag{5}$$

where the first term on the right hand side is the incoming shortwave radiation K, the second is the incoming longwave radiation L_{in}, and the third term is the outgoing longwave radiation L_{out}. ϵ_w (no units) is the effective emissivity of dew water, ϵ_l (no units) is the effective emissivity of the dry leaf, ϵ_{atm} (no units) is the effective emissivity of the atmosphere defined as (Kustas et al., 1527): $\epsilon_{atm} = 0.642(e_c(T_{air})/(T_{air} + 273.2))^{1/7}$, and ϵ_{surr} (no units) is the effective

emissivity of the surroundings as seen by the abaxial side of the leaf and is here taken to be equal to ϵ_l. α_{dew} and α_{dry} are the albedo of a wet and a dry leaf (no units), respectively, σ is the Stefan-Boltzman constant in $W\,m^{-2}\,K^{-4}$, and T_{air} is the temperature of the air in °C. For simplicity, the difference in albedo between wet and dry leaves is treated categorically rather than a function of dew amount. A list of parameters is available in Table 1.

Using the Penman–Monteith equation, the evaporative cooling from transpiration is described as (Rodriguez-Iturbe and Porporato, 2004):

$$\lambda E\ =\ 0.622\ \rho_{air}\ g_v\ \lambda_v\ \frac{e_{sat}(T_{leaf})\ -\ e_c(T_{air})}{P}, \tag{6}$$

where ρ_{air} is the density of air in $kg\,m^{-3}$, P is the atmospheric pressure in Pa, e_{sat} is the saturation vapor pressure in Pa, e_c is the vapor pressure in Pa, λ_v is the latent heat of vaporization in $J\,kg^{-1}$ defined as a function of temperature (in °C) as (Dingman, 2002): $\lambda_v\ =\ 10^6\ \times\ (2.5\text{–}2.36 \times 10^{-3} \times T)$, and g_v is the total conductance defined as:

$$g_v\ =\ \frac{g_h\ g_s}{g_h\ +\ g_s}, \tag{7}$$

with g_s the stomatal conductance and g_h the conductance of the boundary layer to water vapor, all three expressed in $m\,s^{-1}$. The conductance of the boundary layer can be described as a function of the heat transfer coefficient, h_c (Incropera et al., 2007; Schymanski et al., 2013):

$$g_h\ =\ \frac{h_c}{\rho_{air}\ C_a\ N_{Le}^{2/3}} \tag{8}$$

with C_a is the heat capacity of air, equal to $1010\ J\,kg^{-1}\,K^{-1}$. N_{Le} is the dimensionless Lewis number, defined as the ratio of thermal diffusivity to mass diffusivity: $N_{Le}\ =\ \frac{\alpha_a}{D_{va}}$, with α_a the thermal diffusivity of air ($m^2\,s^{-1}$) depending on the boundary layer temperature $T_b = (T_{air} + T_{leaf})/2$ as: $\alpha_a = (T_b + 273.2)\ 1.32 \times 10^{-7} - 1.73 \times 10^{-5}$ and D_{va} is the diffusivity of water vapor in air ($m^2\,s^{-1}$): $D_{va} = (T_b + 273.2)\ 1.49 \times 10^{-7} - 1.96 \times 10^{-5}$. The heat transfer coefficient h_c ($W\,K^{-1}\,m^{-2}$) can be described as:

Table 1
List of parameters used in Section 2.

Parameter	Value	Unit	Description	Relevant equations
α_{dew}	0.1		Albedo of a wet leaf	(5)
α_{dry}	0.5		Albedo of a dry leaf	(5)
ϵ_w	0.97		Emissivity of water	(5)
ϵ_l	0.95		Emissivity of a dry leaf	(5)
γ_0	34.6×10^{-6}	$mol\,mol^{-1}$	CO_2 compensation point at T_0	(15)
γ_1	0.0451	K^{-1}		(15)
γ_2	0.000347	K^{-2}		(15)
ρ_{air}	1.225	$kg\,m^{-3}$	Density of air	(6), (8), (18)
σ	5.670373×10^{-8}	$W\,m^{-}\,K^{-4}$	Stefan–Boltzmann constant	(5)
c_{air}	400×10^{-6}	$mol\,mol^{-1}$	CO_2 concentration of air	(12), (20)
C_a	1005	$J\,kg^{-1}\,K^{-1}$	Heat capacity of air	(8)
C_l	3750	$J\,kg^{-1}\,K^{-1}$	Leaf heat capacity	(4)
C_d	4181.3	$J\,kg^{-1}\,K^{-1}$	Heat capacity of liquid water	(4)
H_{kc}	59 430	$J\,mol^{-1}$	Activation energy for K_c	(27)
H_{ko}	36,000	$J\,mol^{-1}$	Activation energy for K_o	(27)
H_{vv}	116,300	$J\,mol^{-1}$	Activation energy for $V_{c,max}$	(26)
H_{dv}	202,900	$J\,mol^{-1}$	Deactivation energy for $V_{c,max}$	(26)
H_{vj}	79,500	$J\,mol^{-1}$	Activation energy for J_{max}	(29)
H_{dj}	201,000	$J\,mol^{-1}$	Deactivation energy for J_{max}	(29)
$J_{max,0}$	17.6	$J\,m^{-2}$	Electron transport capacity at T_0	(29)
$K_{c,0}$	302×10^{-6}	$mol\,mol^{-1}$	Michaelis–Menten coefficients for CO_2 at T_0	(27)
$K_{o,0}$	256×10^{-3}	$mol\,mol^{-1}$	Michaelis–Menten coefficients for O_2 at T_0	(27)
M_{H_2O}	0.0182	$kg\,mol^{-1}$	Molar mass of water	(19)
N_{Pr}	0.71		Prandtl number for air	(10)
O_c	0.21	$mol\,mol^{-1}$	Oxygen mole fraction in chloroplast	(23)
R	8.314	$J\,mol^{-1}\,K^{-1}$	Ideal gas constant	(13), (21), (25)
S_v	650	$J\,mol^{-1}$	Entropy term	(26), (29)
T_0	293.2	K	Reference temperature	(15), (26)
$V_{c,max,0}$	50×10^{-6}	$mol\,m^{-2}\,s^{-1}$	Maximum carboxylation rate at T_0	(25), (26)

$$h_c = k_a \frac{N_{Nu}}{L_l}, \tag{9}$$

where k_a is the thermal conductivity of air in the boundary layer in $W\,K^{-1}\,m^{-1}$ described as (Schymanski et al., 2013): $k_a = (T + 273.2) \times 6.84 \times 10^{-5} + 5.62 \times 10^{-3}$, L_l is the characteristic length of the leaf in m, taken to be equal to the leaf width (Schymanski and Or, 2016), and N_{Nu} is the dimensionless Nusselt number, the ratio of convective to conductive heat transfer across the boundary layer:

$$N_{Nu} = 0.664\, N_{Re}^{1/2}\, N_{Pr}^{1/3}, \tag{10}$$

with N_{Pr} the dimensionless Prandtl number, equal to 0.71 for air, and N_{Re} is the Reynolds number, defined as the ratio of inertial forces to viscous forces within a fluid:

$$N_{Re} = \frac{u\, L_l}{\nu_{air}}, \tag{11}$$

with u the wind velocity in $m\,s^{-1}$, and ν_{air} is the kinetic viscosity of the air in $m\,s^{-1}$, here taken to be a function of temperature using the empirical relation (Schymanski et al., 2013): $\nu_{air} = (T + 273.2) \times 9 \times 10^{-8} - 1.13 \times 10^{-5}$.

For the description of the stomatal conductance, we use an optimized expression of g_s. Optimized stomatal conductance models aim at reflecting the conflict between increased carbon uptake and limited water losses in plants (Wolf et al., 2016). In these models, stomatal conductance is usually described as a function of carbon assimilation, A_n, atmospheric CO_2 concentration, c_{air}, and water vapor deficit (VPD), D as a function of $\frac{A_n}{c_{air}\sqrt{D}}$ (Vico et al., 2013; Medlyn et al., 2011). Although fairly new, these models have been overall very performant in describing stomatal response to environmental conditions during the day (Lloyd and Farquhar, 1994; Dewar et al., 2017). Here, we choose (Vico et al., 2013) expressions for optimized stomatal aperture, $g_{s,mol}$ (expressed in $mol\,m^{-2}\,s^{-1}$) under rubisco and RuBP regeneration limitations:

$$g_{s,mol} = \begin{cases} \frac{A_n}{c_{air}\sqrt{D}} \sqrt{\frac{c_{air}}{1.6\,\lambda_m}}, & \text{if } D > 0 \text{ and } A_n > 0, \text{ under rubisco limitation} \\ \frac{A_n}{c_{air}\sqrt{D}} \sqrt{3 \times \frac{1.6\,\Gamma^*}{\lambda_m}}, & \text{if } D > 0 \text{ and } A_n > 0, \text{ under RuBP regeneration limitation} \\ 0, & \text{otherwise} \end{cases} \tag{12}$$

Stomatal conductance in $mol\,m^{-2}\,s^{-1}$ can then be transformed to $m\,s^{-1}$ as:

$$g_s = \frac{R\, T_{leaf,K}}{P}\, g_{s,mol} \tag{13}$$

In this expression, A_n is expressed in $mol\,m^{-2}\,s^{-1}$ and described later in Eq. (31), c_{air} is the CO_2 concentration of air, set here to $400 \times 10^{-6}\,mol\,mol^{-1}$, and λ_m is the marginal water use efficiency taken to be: $\lambda_m = \lambda_{m,0}\frac{c_{air}}{c_{air,0}}$ with $c_{air,0} = 380 \times 10^{-6}\,mol\,mol^{-1}$ and $\lambda_{m,0} = 400 \times 10^{-6}\,mol\,mol^{-1}$ (Vico et al., 2013). D (no unit) is defined as:

$$D = \max\left(0, \frac{e_{sat}(T_{leaf}) - e_c(T_{air})}{P}\right) \tag{14}$$

with P, e_{sat}, and e_c as described above. Finally, Γ^* is the CO_2 compensation point ($mol\,mol^{-1}$) calculated as a function of leaf temperature $T_{leaf,K}$ in K as:

$$\Gamma^* = \gamma_0\, [1 + \gamma_1(T_{leaf,K} - T_0) + \gamma_2(T_{leaf,K} - T_0)^2]. \tag{15}$$

The sensible heat flux in and out of the leaf is described as:

$$H = 2\, h_c\, (T_{leaf} - T_{air}), \tag{16}$$

which is positive (energy flux out of the leaf) when the leaf is hotter than the ambient air, and negative (flux into the leaf) when the leaf is cooler than the air. Finally, when dew is present, the latent energy dissipated from evaporating dew or accumulated from condensing dew is:

$$P_{lat} = \begin{cases} \lambda_v(T_{leaf})\, \frac{dm_d}{dt}, & \text{if } \frac{dm_d}{dt} > 0 \\ \lambda_c(T_{leaf})\, \frac{dm_d}{dt}, & \text{if } \frac{dm_d}{dt} < 0 \end{cases} \tag{17}$$

with m_d the dew mass (kg) and λ_c the latent heat of condensation ($J\,kg^{-1}$) and is equal to λ_v. The dew mass balance can be written as follows:

$$\frac{d\, m_d}{dt} = 0.622\, S_l\, \rho_{air}\, g_h\, \left[\frac{e_c(T_{air}) - e_{sat}(T_{leaf})}{P}\right], \tag{18}$$

Note that in Eq. (18), the e_{sat} and the e_c have opposite signs compared to the expression of transpiration (Eq. (6)) because we are counting dew *condensation* positively and *evaporation* negatively.

2.1.2. Modeling net assimilation

Water use efficiency (WUE) is the ratio of CO_2 flux into the leaf over the water vapor flux out of the leaf:

$$WUE = \frac{A_n}{E_{mol}}, \tag{19}$$

where E_{mol} is the transpiration flux expressed in $mol\,m^{-2}\,s^{-1}$ and which is easily calculated from λE as described in Eq. (6): $E_{mol} = \frac{\lambda E}{\lambda_v\, M_{H_2O}}$, with M_{H_2O} the molar mass of water equal to $0.0182\,kg\,mol^{-1}$. For A_n, the net flux of CO_2 ($mol\,m^{-2}\,s^{-1}$) we use the model described in (Rodriguez-Iturbe and Porporato, 2004):

$$A_n = g_{sba}\, (c_{air} - c_i), \tag{20}$$

where c_i is the intercellular CO_2 concentration within the leaf ($mol\,mol^{-1}$), and g_{sba} ($mol\,m^{-2}\,s^{-1}$) is the equivalent conductance corresponding to the stomatal (g_s), boundary layer (g_h), and mesophyll (g_m) conductances to CO_2 put in series:

$$g_{sba} = \frac{1}{\frac{1.6\,R\,T_{leaf,K}}{g_s\,P} + \frac{1.37\,R\,T_{leaf,K}}{g_h\,P} + \frac{1}{g_m}} \tag{21}$$

with atmospheric pressure P in Pa, $T_{leaf,K}$ the leaf temperature in K, and g_h and g_s the boundary layer and stomatal conductances to water vapor expressed in $m\,s^{-1}$ and as described in Eqs. (8) and (13), respectively. The mesophyll conductance to CO_2 can be described as a function of leaf temperature using the following empirical relation (Buckley et al., 2014):

$$g_m = 0.18\, \exp\left[0.71027\, \ln\left(\frac{T_{leaf}}{36.75}\right)^2\right] \tag{22}$$

with T_{leaf} in °C and g_m in $mol\,m^{-2}\,s^{-1}$. In addition, A_n can also be described as the minimum of the rubisco-limited and the light-limited assimilation rates. The rubisco limitation can be described as (Rodriguez-Iturbe and Porporato, 2004):

$$A_{n,c} = V_{c,max}\, \frac{c_i - \Gamma^*}{c_i + K_c\,(1 + O_c/K_o)} - R_l, \tag{23}$$

and the RuBP regeneration limitation caused by light limitation:

$$A_{n,q} = J\, \frac{c_i - \Gamma^*}{4\,(c_i + 2\Gamma^*)} - R_l, \tag{24}$$

Γ^* is the CO_2 compensation point ($mol\,mol^{-1}$) calculated as a function of leaf temperature as described in Eq. (15). R_l ($mol\,m^{-2}\,s^{-1}$) is the non-photorespiratory CO_2 release in the light and is calculated as a function of leaf temperature following the expression (Schymanski and Or, 2016):

$$R_l = 0.0089\, V_{c,max,0}\, \exp\left[18.72 - \frac{46.39}{10^{-3}\,R\,T_{leaf,K}}\right] \tag{25}$$

$V_{c,max}$ is the maximum carboxylation rate ($mol\,m^{-2}\,s^{-1}$) described as:

$$V_{c,max} = V_{c,max,0} \frac{\exp\left[\frac{H_{vv}}{RT_0}\left(1 - \frac{T_0}{T_{leaf,K}}\right)\right]}{1 + \exp\left[\frac{S_v\, T_{leaf,K} - H_{dv}}{R\, T_{leaf,K}}\right]}, \tag{26}$$

K_c and K_o are the Michaelis–Menten coefficients ($mol\,mol^{-1}$) for CO_2 and O_2, respectively and are described as (where x is either c or o):

$$K_x = K_{x,0}\, \exp\left[\frac{H_{k_x}}{RT_0}\left(1 - \frac{T_0}{T_{leaf,K}}\right)\right]. \tag{27}$$

J is the electron transport rate given by the lower root of the quadratic equation:

$$\kappa_1 J^2 - (\kappa_2 Q + J_{max})J + \kappa_2\, Q\, J_{max} = 0, \tag{28}$$

with $\kappa_1 = 0.95$, $\kappa_2 = 0.25$ and,

$$J_{max} = J_{max,0} \frac{\exp\left[\frac{H_{vj}}{RT_0}\left(1 - \frac{T_0}{T_{leaf,K}}\right)\right]}{1 + \exp\left[\frac{S_v\, T_{leaf,K} - H_{dj}}{R\, T_{leaf,K}}\right]}, \tag{29}$$

and Q ($mol\,photons\,m^{-2}\,s^{-1}$) the absorbed photon irradiance, which can be calculated from incoming shortwave radiation as (Buckley et al., 2014; Schymanski and Or, 2016): $Q = 10^{-6} \times \frac{(1-\alpha)\, R_{sw}}{0.5666}$, with α taken to be either α_{dew} or α_{dry} depending on whether dew is present or not.

To calculate A_n, we replace c_i in Eqs. (23) and (24) by its expression derived from Eq. (20). Isolating A_n, we obtain two expressions for $A_{n,c}$ and $A_{n,q}$ (Schymanski and Or, 2016)

$$A_{n,c} = \left(c_{air} + K_c\left(1 + \frac{O_c}{K_o}\right)\right)\frac{g_{sba}}{2} - \frac{R_l}{2} + \frac{V_{c,max}}{2}$$
$$- \frac{1}{2}\sqrt{\left(\left(c_{air} + K_c\left(1 + \frac{O_c}{K_o}\right)\right)g_{sba} + R_l\right)^2 - \left(2\left(c_{air} - K_c\left(1 + \frac{O_c}{K_o}\right) - 2\Gamma^*\right)g_{sba} + 2R_l - V_{c,max}\right)V_{c,max}}$$

$$A_{n,q} = (c_{air} + 2\Gamma^*)\frac{g_{sba}}{2} - \frac{R_l}{2} + \frac{J}{8}$$
$$- \frac{1}{8}\sqrt{16((c_{air} + 2\Gamma^*)\,g_{sba} + R_l)^2 - (8\,(c_{air} - 4\Gamma^*)\,g_{sba} + 8R_l - J)\,J} \tag{30}$$

and

$$A_n = \min(A_{n,c},\ A_{n,q}) \tag{31}$$

2.2. Model testing

To test the dew deposition and evaporation components of the derived model, we considered a suite of data collected on a leaf wetness sensor network deployed at the Blue Oak Ranch Reserve near San Jose, California. Leaf wetness sensors were originally developed to identify risks of plant foliar disease under wet leaf conditions (Chungu et al., 2001; Dalla Marta et al., 2005, 2007; Rossi et al., 2008; Gil et al., 2011). Contemporary leaf wetness sensors mimic key thermodynamic and

surface properties of leaves such as hydrophobicity and total heat capacity. They have a dielectric constant that is altered by the presence of water on the sensor surface (Letts and Mulligan, 2005; Gil et al., 2011; Berkelhammer et al., 2013). The dielectric constant can be calibrated against the mass of water on the sensor surface for a given excitation voltage, providing quantitative information about water inputs and leaf-level storage (Cobos, 2013). What remains unclear is the robustness of the relationships between the sensor output, the evolution of the water mass on the sensor surface, and the water mass present on plant leaves under the same conditions. Thus, before interpreting the leaf wetness sensor network outputs in terms of masses of water accumulating on the sensors – and thus potentially surrounding plant leaves – a calibration experiment is necessary.

2.2.1. Field data

An array of over 57 wireless sensor nodes is deployed at the Blue Oak Ranch Reserve (BORR), a Biological Field Station and Ecological Reserve located near San Jose, California (Hamilton et al., 2011). Leaf wetness data, air temperature and relative humidity are reported together at 25 of the 57 nodes, with 15 minutes resolution (Fig. S1 in the Supporting Information). Data is collected and transmitted wirelessly using an eKo Pro wireless network (eK2120, MEMSIC, Inc, Andover, MA). Leaf wetness sensors were installed progressively from late 2012 through 2014. Incoming solar radiation, wind speed, rainfall, and atmospheric pressure are available hourly at six weather stations beginning operation in 2010. Because BORR experiences fog events in addition to dew, 2011–2013 web camera pictures taken from the Lick Observatory, situated on the summit of Mount Hamilton, were used to classify time periods when fog was visible over the reserve. Images were taken every 15 min. Eight categories of imagery were used in the classification, including dark, fog, clear day, or lens obscured. Foggy days were separated into conditions suitable for radiation or advection fog based on wind speed and leaf wetness patterns. Radiation fog forms under low windspeed conditions ($< 2.23\,m\,s^{-1}$), and is controlled by similar physics to that of to dew formation. Leaf wetness sensor output during the classified radiation fog events were similar to those observed for dew events. They were characterized by a single wetting event, with a a slow water deposition phase and a rapid drying phase (Fig. 1). Advection fog is usually accompanied by higher windspeed and generates multiple small drying and rewetting events. To test the dew model, we focused on five leaf wetness sensors that had data overlapping the fog classification data and low data gap percentage. We included both dew events and conditions when radiative fog occurred in the model testing. The data is available online through the UC Berkeley Sensor Database website (http://sensor.berkeley.edu/aboutDB.html).

2.2.2. Leaf wetness sensor calibration

Calibration experiments were conducted within a a $30 \times 50 \times 50\,cm$ plexiglass chamber with a removable front panel. At
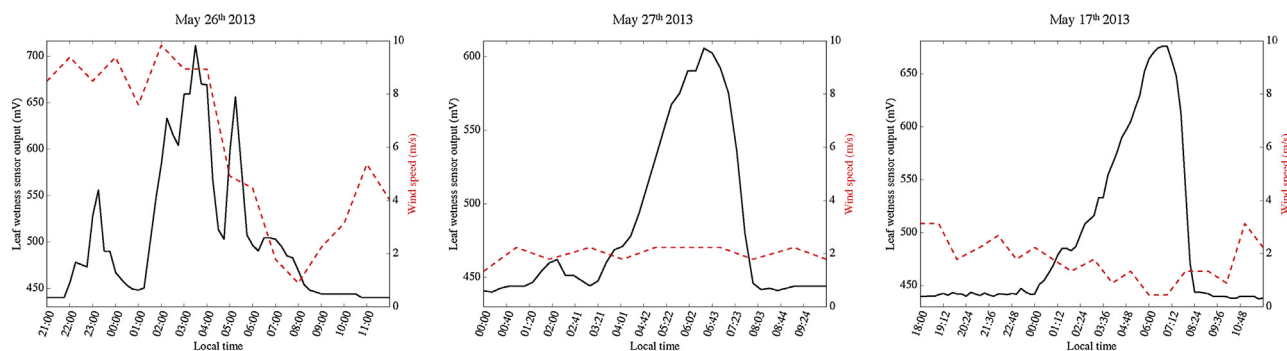

Fig. 1. Leaf wetness sensor (black solid line) and windspeed (red dotted line) data for three different water deposition events: advection fog on the left, radiation fog in the center, and dew on the right. (For interpretation of the references to color in this figure legend, the reader is referred to the web version of the article.)

the bottom of the panel, an ultrasonic mist generator (NHKR, M-011) with > 300 mL/h capacity was floated in a water reservoir, and covered with a wire screen to prevent water splashing from the reservoir into the chamber. Mist generated at the bottom of the chamber was dispersed using a waterproof fan (JSarci, Scenario 120). A dielectric leaf wetness sensor (Decagon, 40020) was mounted horizontally 30 cm above the floor of the chamber (c. 27 cm above the reservoir water surface), run using an excitation voltage of 3000 mV, and reported continuously to a datalogger (Campbell CR1000).

Leaves of *Quercus douglasii* (blue oak) and *Quercus lobata* (valley oak) were placed horizontally one at a time within the wire cradle in a dry chamber. These two species were chosen because they are commonly found at the BORR research station. The wire cradle was suspended at the same level as the leaf wetness sensor. The cradle was suspended from a load cell (Measurement Specialties, Inc., FN3280) located outside the chamber. Mass readings from the load cell were continuously logged throughout the experiment, and the load cell was calibrated at the beginning and end of each experimental run. Once the load cell readings stabilized, the ultrasonic mist generator and fan were started, the chamber was sealed, and the load cell and wetness sensor readings logged over 45 min. Visually, the chamber reached a homogeneously 'foggy' condition within 45 s of starting the experiment. While the experiment ran, we measured the dry weight of a polyvinyl alcohol cloth. At the conclusion of the experiment, we swabbed both surfaces of the leaf wetness sensor with the cloth and weighed the cloth to estimate the mass of water accumulated on the sensor.

We measured the surface area of the tested leaves as follows: the leaves were firstly flattened and fastened to a white background with a one cm^2 reference square marked on it in black. The sheets were scanned in an optical scanner, converted to a binary (black and white image) and the black pixel count associated with the leaf used to estimate the surface area. Seven and eight different leaves were tested for for *Q. douglasii* and *Q. lobata*, respectively. Control runs were also made with no leaf in place to allow the mass change associated with fog deposition on the cradle to be determined. The mass changes in the absence of leaves were negligible, suggesting that no significant deposition of water on the wire cradle occurred.

The logged data were subjected to a series of quality assurance steps. The mass calibration performed at the beginning and end of each trial was used to correct for sensor drift during the trial by imposing a linear drift term that was subtracted from the measured data. 95% confidence intervals on the load cell measurements were made based on
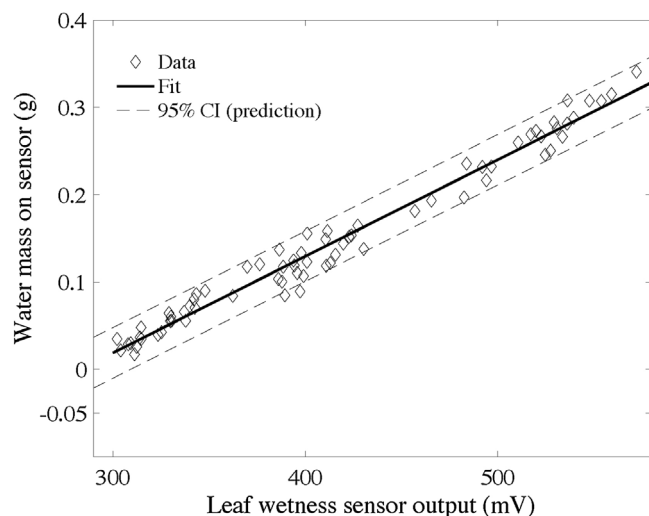
repeat measures, and propagated into all subsequent computations using the R qpcR package. Where the total mass of water accumulated on the leaf surface during the experimental trial fell within the 95% confidence interval for the leaf dry mass (i.e. a low signal to noise ratio, primarily occurring on leaves with a small surface area), the data was excluded from subsequent analysis.

2.3. Model experiments

We first look at the influence of leaf size and dew deposition amount on transpiration and CO_2 assimilation. Meteorological data for a typical day at BORR were chosen (Fig. S2 in the Supporting Information) and the model was run for different characteristic leaf lengths, L_1 (Eq. (9)). We vary the dew deposition amount at dawn and model transpiration and assimilation during a full diurnal cycle. We compare these results to the transpiration and assimilation of a dry leaf in the same environmental conditions.

We then explore the effects of a changing climate by varying relative humidity, wind speed and air temperature. We use the diurnal time series of air temperature, pressure, and solar radiation presented above (Fig. S2 in the Supporting Information) and run the model for a set of wind speeds from 0.1 to 5 m s^{-1} and relative humidities from 1 to 100%. Relative humidity and windspeed are kept constant for the entire diurnal cycle. We set the dew deposition amount at dawn to 0.4 kg/m^2 and calculate the decrease in transpiration and CO_2 assimilation associated with the presence of dew, compared to diurnal transpiration and assimilation levels of a dry leaf. We also record leaf wetness duration. To reproduce the warming expected in the Tropics by the end of the 21st century (Cook et al., 2014), we repeat the experiment with an air temperature 5 °C higher than recorded air temperature. The experiment is conducted for leaf characteristic lengths L_1 (Eq. (9)) of 1 and 50 cm.

3. Results and discussion

3.1. Laboratory leaf wetness measurements

Fig. 2 shows a scatter plot of the mass of water deposited on the leaf wetness sensor at the end of the experimental runs and the voltage output from the sensor recorded at the same time period. The strong linear trend between the water mass on the sensor and the output, had a coefficient of determination of 0.98 and was well described by the following relationship:

$$M = (1.11 \times 10^{-3} \pm 34.20 \times 10^{-5}) \text{ LWS} - (0.313 \pm 1.8 \times 10^{-2}) \tag{32}$$

where M is the total mass of water deposited on the leaf wetness sensor (g), and LWS represents the output from the leaf wetness sensor in mV. Error terms indicate the 95% confidence intervals that would apply to predictions made with this fit, and indicate that the mass of water accumulating on the leaf wetness sensor could be estimated from the output voltage with an error of approximately 5%. The experimental results agree with previous analyses comparing sensor water accumulation to sensor output (Cobos, 2013) and indicate that the dielectric sensor provided robust detection of leaf mass changes on the sensor surface. Unlike previous results (Cobos, 2013), all data used in developing this relationship were derived from (i) independent experimental runs, and (ii) from the ambient deposition of mist droplets on the sensor surface, rather than a sprayed application of water to the sensor surface. We postulate that these conditions may be more representative of field conditions induced by fog or dew formation than direct spraying.

Water deposition on the real leaves shows a strong linear relationship with water on the leaf wetness sensor (Fig. 3) under the same conditions. Overall, we find that the leaf wetness sensor and the leaves accumulate c. the same amount of water, but the leaf wetness sensor appears to systematically underestimate the amount of water
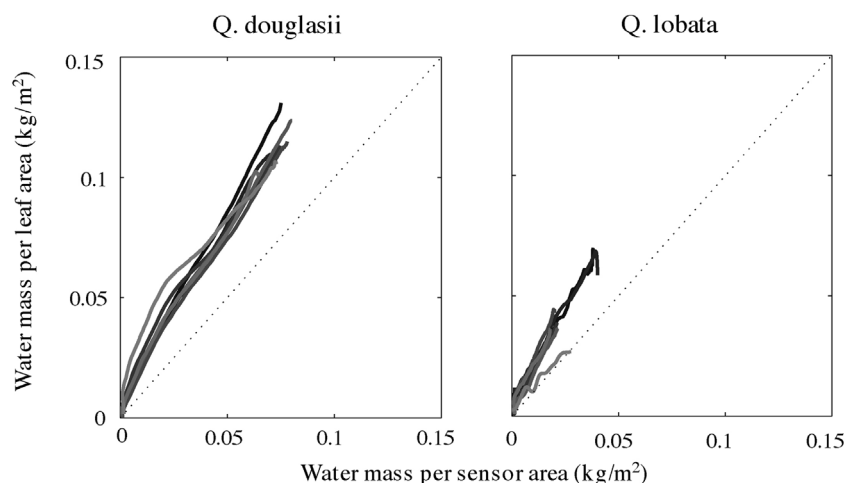

Fig. 2. Calibration curve for the mass of deposited water on the leaf wetness sensor as a function of the voltage reported by the leaf wetness sensor. The relationship was strongly linear and well described ($R^2 = 0.97$) by the function: Mass(g) = 1.105×10^{-3} Voltage(mV) − 0.3126.

Fig. 3. Water accumulated on the leaf wetness sensor and on real leaves of *Quercus douglasii* and *Quercus lobata*. The different shades of grey show the different trials done using different leaves of each species ($n = 7$ for *Q. douglasii* and $n = 8$ for *Q. lobata*).

accumulated on real leaves. These differences are likely linked to differences in leaf heat capacity and surface properties that are improperly reproduced by the sensor.

3.2. Testing the dew model against field data

The dew deposition model was tested using field data for 16 different dew and radiative fog events at all 5 sensors. Field data for air temperature, relative humidity, incoming solar radiation, wind speed, and atmospheric pressure were used as input in the model. The data was linearly interpolated to 1s time resolution. The model solved for leaf temperature and dew amount, and dew accumulation was compared to estimated accumulation from the leaf wetness sensors. Eq. (32) was adapted to the field sensors, which all showed a baseline (mV output for dry sensor) of 0.4884, instead of 0.313 as described in Section 3.1. This is due to the difference in datalogger used and does not affect the measurement (Chris Chambers, Meter Group, Inc., personal communication). Model performance was estimated using an absolute root-mean-square error (RMSE), and relative RMSE (normalized by the maximum recorded leaf wetness). Results are shown in Table 2.

The model was generally in very good agreement with the recorded leaf wetness, capturing the timing of dew deposition, and the amount deposited (Fig. 4). While only a limited number of dew event were available, the model represented these events better that radiative fog events (Table 2, average RMSE/normalized RMSE for dew events: 0.018/0.42; fog events: 0.045/0.79), likely because some subtleties of radiative fog formation, such as aerosol concentration (Yamaguchi et al., 2013) or fog water content (Katata et al., 2011), are omitted from the model. The model errs towards overestimating the amount of water deposited on the sensor. This is consistent with the results observed in our laboratory experiment, where leaf wetness sensor deposition was systematically lower than water accumulating on real leaves (Fig. 3). In addition to issues with the inherent design of the leaf wetness sensor, there might also be additional explanations for this: (1) the model aims at representing a real, transpiring leaf, whereas the leaf wetness sensor is an unanimated object. Leaf transpiration will decrease leaf temperature further than what would be expected for the leaf wetness sensor. However, for all the dew and radiation fog events observed in the data, the water deposition started at night, when stomata are shut, limiting the effect of this potential source of error. (2) Sensor placement: in the field, the leaf wetness sensors are attached to the radiation shield (see Fig. S1 in the Supporting Information). The sensors are therefore in thermal equilibrium with the radiation shield, which is likely to be generally warmer than what the leaf wetness sensor would have been if it had been installed in suspension, like a real leaf. This will

therefore lead to lower-than-expected water deposition amount on the sensor which are not captured by the model.

3.3. Model predictions

3.3.1. Leaf size effects on transpiration and assimilation

Transpiration suppression in leaves lasts until dew evaporates, which depends on evaporation rate and on the amount of dew accumulated before sunrise. We find that transpiration suppression over the course of a day (Fig. S2) is near-linearly correlated with dew amount for all leaves sizes (Fig. 5). Unexpectedly, we find that carbon assimilation is also decreased by the presence of dew (Fig. 6), and that for small leaves, the decrease follows a similarly linear relationship to what was found for transpiration. In addition, both transpiration and assimilation are further decreased in larger leaves, likely because larger leaves stay wet longer, thanks to a deeper boundary layer that effectively reduces dew evaporation. The effect of dew deposition on the assimilation in larger leaves appears to level off for dew amounts larger than c. 0.6 kg/m². This non-linearity is linked to midday stomatal closure in larger leaves (Fig. S2), likely due to high leaf temperature and low relative humidity in the middle of the day (Tenhunen et al., 1981). Finally, we find that WUE is not affected by the presence of dew (data not shown).

3.3.2. Effects of climatic changes

In Fig. 7, we show how wind speed, relative humidity, and leaf characteristic length impact transpiration, CO_2 assimilation, and dew duration. As expected, for small leaves, high relative humidity is associated with an increase in transpiration and CO_2 assimilation suppression, which corresponds with longer leaf wetness duration. In the limit of RH = 100% and when T_{air} and T_{leaf} are equal, as it is often the case in the early morning, dew is not excepted to evaporate at all, with leaf wetness lasting multiple hours. Similarly, lower wind speed leads to higher decrease in transpiration because of the associated increase in boundary layer thickness (Eq. (8)), which increases the diffusion time of water vapor out of the boundary layer. CO_2 assimilation is also decreased at low windspeeds for small leaves.

In large leaves (Fig. 7, bottom row) we actually observe an increase in transpiration and CO_2 assimilation at low windspeed. This is again likely linked to an increase in stomatal conductance due to the presence of dew at mid-day, when larger leaves would usually close their stomata (Figs. 5, 6, and S2). At high relative humidity and windspeed below 1 m s⁻¹, we find an increase in assimilation that also corresponds to a decrease in transpiration. This will therefore lead to an overall increase in water use efficiency (Eq. (19)). This domain of optimal dew effect is associated with an increase in CO_2 assimilation of up to c. 20% and a
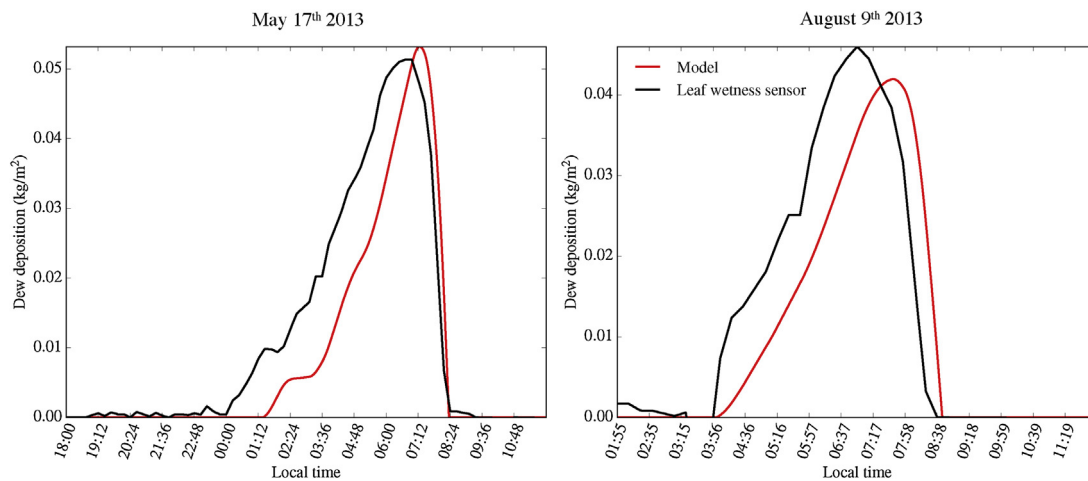
Fig. 4. Modeling dew formation for two dew events at the Blue Oak Ranch Reserve in California. The red line shows the modeled dew amount, obtained from air temperature, wind speed, relative humidity, solar radiation, and atmospheric pressure data. The black line shows the leaf wetness sensor output at the site, with the mV output transformed to dew amount using the relation from Section 3.1. (For interpretation of the references to color in this figure legend, the reader is referred to the web version of the article.)

decrease in transpiration by about 15%. Interestingly, this effect does not appear in smaller leaves (Fig. 7, top row). Fig. S3 (in Supporting Information) explores the effect that an increase of air temperature by 5 °C would have on transpiration, assimilation and dew duration. Overall, the patterns observed are similar to the ones in Fig. 7, but a clear decrease in the effects of dew is seen, with a general decrease in transpiration and CO_2 assimilation reduction by about 5 percentage points.

3.4. Implications

Dew deposition is a phenomenon that is commonplace across most ecosystems on the planet (Vuollekoski et al., 2015). A large knowledge gap exists in vegetation response to a changing climate (Fisher et al., 2017; Kooperman et al., 2018), and as dew frequency and amount are expected to be affected by climate change (Vuollekoski et al., 2015; Tomaszkiewicz et al., 2016), understanding the effects of these changes for plants growing in areas of common dewfall may become even more important. Our results point at significant water savings from transpiration suppression of up to a 25% decrease from daily transpiration levels, in particular for bigger leaves with L_l around 50 cm (Fig. 5). At low wind speed, bigger leaves might even experience a combined decrease in transpiration and increase in assimilation leading to an increase in WUE (Fig. 7). Leaves this size are common in tropical areas,

where high relative humidity leads to common dew deposition (Lakatos et al., 2012; Aparecido et al., 2017). Such levels could also have a significant impact on plant transpiration in the case of drought which is a big unknown in our understanding of vegetation response to a changing climate (Fisher et al., 2017). However, leaves under low water potential are likely to close their stomata to prevent cavitation (Rodriguez-Dominguez et al., 2016), which would then eliminate transpiration along with any potential effect from dew through transpiration suppression. The drought level at which stomata closure will happen is highly dependent on the species (Brodribb and Holbrook, 2003) and the model proposed here can easily be modified to explore the effects of dew on different species and in different types of ecosystems.

The negative impact of dew on carbon assimilation, which experiences up to 10% decrease under high dewfall, is mostly due to stomata closure under (1) decreased incoming radiation which affects assimilation by decreasing the absorbed photon irradiance, Q and therefore J through Eq. (28), and (2) low leaf temperatures that are extended after sunrise when the leaf is covered in dew. In the case of amphistomatous leaves, dew might also directly affect CO_2 concentration in the chloroplasts by obstructing part of the stomata and hindering CO_2 diffusion. Here, we model the case of a hypostomatous leaf with dew depositing on the adaxial surface, and this third mechanism can therefore be neglected.
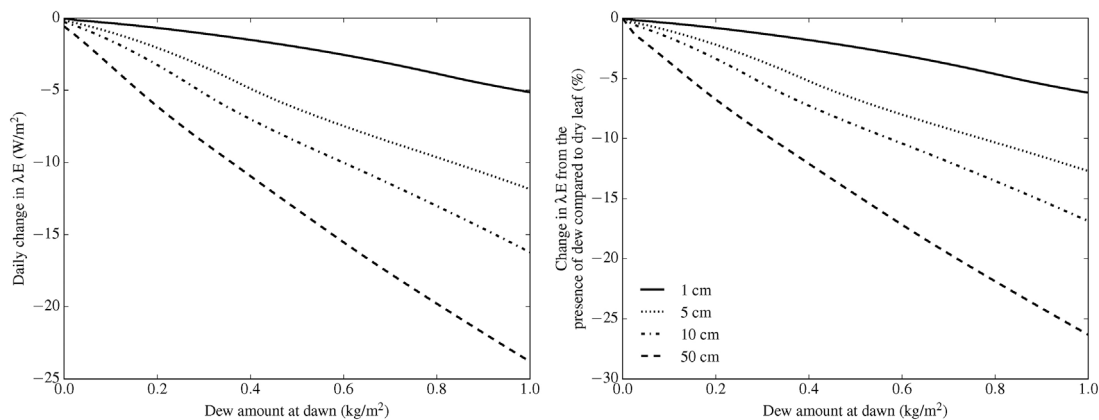
Fig. 5. Left: total daily change in transpiration due to the presence of dew as a function of dew amount present on the leaf at sunrise for four different leaf characteristic lengths, L_l. **Right:** Relative change in daily transpiration due to the presence of dew compared to transpiration in a dry leaf. The environmental parameters used to drive the model are presented in the Supporting Information (Fig. S2).
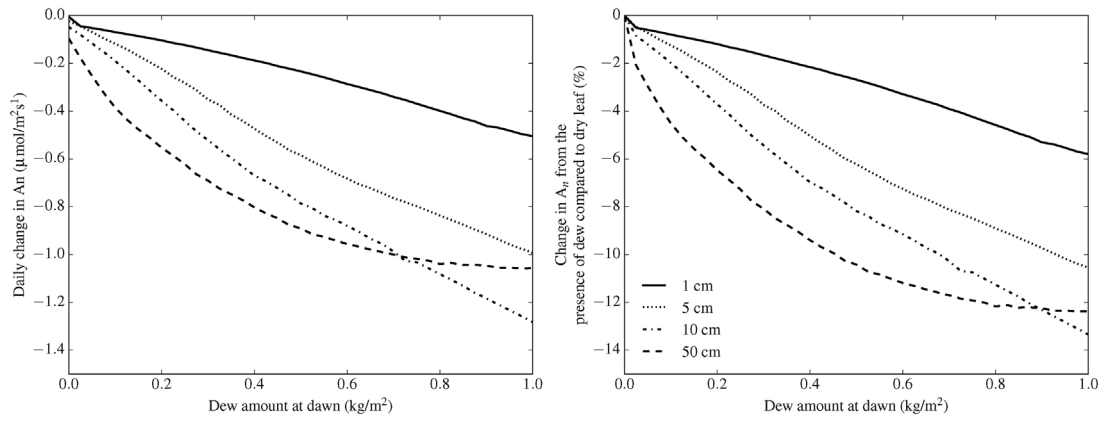
Fig. 6. Left: total daily change in CO_2 assimilation due to the presence of dew as a function of dew amount present on the leaf at sunrise for four different leaf characteristic lengths, L_l. *Right:* Relative change in daily CO_2 assimilation due to the presence of dew compared to assimilation in a dry leaf. The environmental parameters used to drive the model are presented in the Supporting Information (Fig. S2).

One could have expected that transpiration suppression from dew allowed leaves to open up their stomata to uptake CO_2 with little water losses. Our model indicates that this is only the case for large leaves in low windspeed and high relative humidity conditions, and that this positive effect on assimilation does not happen in smaller leaves, although experimental evidence is still needed to confirm this result. However, it is important to note that WUE appears to be mostly unchanged by the presence of dew, showing that transpiration and assimilation are decreased by a similar factor due to the presence of dew.

Finally, the results presented here are also applicable to other phenomena, such as rainfall interception. Thick canopies can intercept the integrity of small rainfall events (Guevara-Escobar et al., 2007; Zimmermann et al., 2013), leading to leaf water deposition at the surface of the leaves much larger than in the case of dew. In addition,

rainfall interception happens primarily in the upper leaves of the plants, which are also the leaves most exposed to the sun and more likely to transpire during the day. This might lead to a transpiration suppression effect larger than what we estimated here for dew. However, dew formation is larger during nights with clear skies. On the opposite, rain clouds will reduce incoming radiation to the leaf, and as a consequence reduce the effects of leaf wetness on transpiration and assimilation compared to that of dew. How these two aspects of rainfall interception would balance out is still unclear, and should be the topic of a more detailed investigation.

One of the main limitations of the present model is that it represents dew deposition as a uniform film of water on top of the leaf. Indeed, dew might also deposit on the abaxial surface of the leaf. However, the emissivity of the surrounding environment seen by the bottom of the
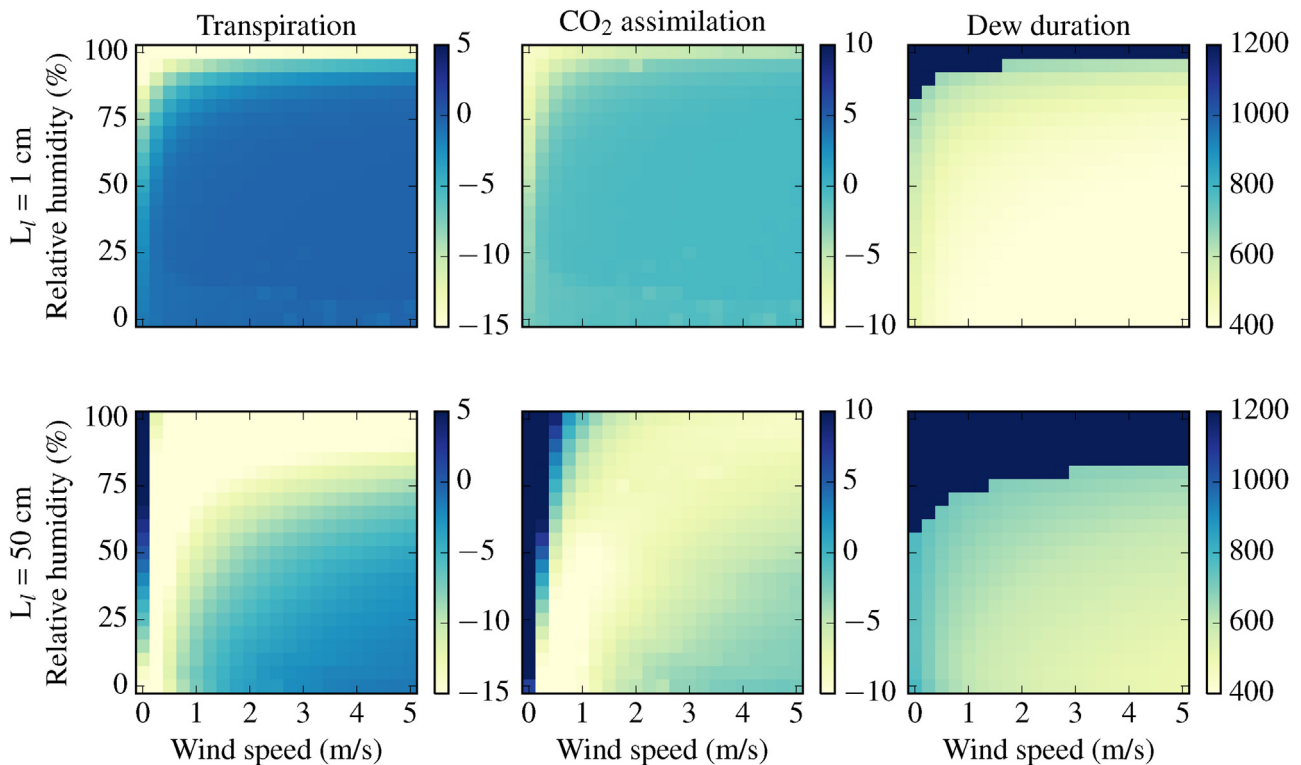
Fig. 7. Expected change in daily transpiration and CO_2 assimilation (% change from daily values in the absence of dew), as well as dew dry-out time (in min since midnight) for varying wind speeds (m s^{-1}) and relative humidity values (%), using the air temperature and solar radiation data presented in Fig. S2 assuming a dew deposition amount at dawn of 0.4 kg/m^2. Top row: L_l = 1 cm, bottom row: L_l = 50 cm. Fig. S3 shows the same plots generated for an air temperature 5 °C higher than the temperature presented in Fig. S2.

Table 2

Table showing the results of the model tested on 16 different dew and fog events at the Blue Oak Ranch Reserve in California. The normalized RMSE shows the RMSE divided by the maximum recorded by the leaf wetness sensor for each event. All times shown are local (Pacific Standard) time.

Date	Type	RMSE	Normalized RMSE	Maximum leaf wetness (kg/m^2)		Time of max. wetness		Time wetting starts		Time wetting ends	
				Sensor	Model	Sensor	Model	Sensor	Model	Sensor	Model
2012/08/31	Fog	0.020	0.43	0.046	0.073	8:30	9:24	4:30	4:21	11:07	11:28
2012/10/13	Fog	0.110	2.35	0.049	0.240	8:30	9:17	23:21	21:00	10:59	11:27
2013/04/02	Fog	0.070	0.72	0.099	0.230	6:00	8:13	19:00	20:24	11:59	10:59
2013/04/25	Fog	0.060	0.79	0.077	0.20	5:16	7:31	20:18	20:41	11:31	10:03
2013/05/17	Dew	0.007	0.14	0.051	0.053	6:43	7:15	0:00	1:22	8:24	8:20
2013/05/22	Dew	0.007	0.31	0.022	0.009	4:33	2:56	23:45	0:58	6:23	4:52
2013/05/23	Dew	0.050	1.05	0.050	0.110	1:40	7:37	21:38	21:51	8:23	9:37
2013/05/27	Fog	0.008	0.39	0.020	0.034	6:43	7:16	3:20	2:06	8:38	8:13
2013/06/19	Fog	0.014	0.25	0.056	0.063	6:57	7:29	2:36	3:37	8:38	8:42
2013/06/26	Fog	0.062	1.02	0.061	0.170	6:45	7:20	0:00	0:00	9:45	9:22
2013/08/09	Dew	0.008	0.17	0.046	0.042	6:57	7:42	3:56	3:59	8:38	8:44
2013/08/26	Fog	0.031	0.58	0.054	0.110	6:57	8:18	2:25	2:29	10:12	10:07
2013/09/05	Fog	0.012	0.32	0.039	0.021	7:26	8:18	1:58	1:57	9:17	9:28
2013/09/30	Fog	0.030	0.35	0.084	0.088	6:30	8:50	19:00	2:40	11:15	10:27
2013/10/30	Fog	0.096	1.87	0.052	0.225	6:00	9:13	20:20	20:17	10:45	11:42
2013/12/19	Fog	0.026	0.41	0.063	0.093	3:45	8:18	21:33	21:30	9:57	10:00

leaf is larger than the emissivity of the clear sky seen by the top of the leaf (see Table 1). Dew deposition is therefore much more frequent on the adaxial surface of the leaf than the abaxial one. In addition, most species have no stomata on their adaxial surface (Aparecido et al., 2017). These two elements combined lead us to the conclusion that modeling dew deposition on the top of the leaf only is valid in most cases. In the case of amphistomatous leaves, dew deposition would clog up the stomata of the adaxial surface. However, the diffusion of CO_2 in water is 10^4 times slower than in air, and wet stomata can therefore be considered to be impermeable to CO_2. Other minor effects, such as free convection for large leaves have been neglected here because it hasn't been found to be a significant heat transfer mechanism in most leaves (Leuning, 1988) and would likely not impact the results significantly.

In addition, a more accurate model would represent dew droplets as half-spheres (Beysens, 1995; Tanaka, 2002; Beysens et al., 2006), with dynamic nucleation processes throughout dewfall and dew re-eva-poration (Beysens, 2005; Leach et al., 2006). These processes vary greatly between species and are complex to model (Goldsmith et al., 2016), but a more precise description of the dew would capture subtleties that might have a large overall effect on transpiration suppression. For example, we expect that spherical drops would increase surface roughness, further deepening the leaf boundary layer, and further decreasing transpiration (Schuepp, 1993). Similarly, we do not account for localized increases in relative humidity due to the re-evaporation of dew on the leaf, or from surrounding leaves. This would again have the net effect of decreasing leaf transpiration. Finally, leaf angle is expected to play a major role in both dew amount and incoming radiation. In this model, we assumed a flat leaf, because dew beading up and rolling off the leaf will be highly dependent on the surface of the leaf: pubescence will increase dewfall and retain dew droplets (Konrad et al., 2014), whereas hydrophobic leaves will have low water retention (Holder, 2012a,b). These subtleties will be exacerbated in non-horizontal leaves and should be taken into account when evaluating the effects of dew deposition for a specific species, but are beyond the scope of this work. Leaves are also known to adopt a more vertical orientation at the hottest hours of the day to decrease incoming radiation from the sun (Ehleringer and Comstock, 1987; King, 1997; Posada et al., 2012). This phenomenon generally occurs in the afternoon (Sellers, 2003), at a time when dew has already evaporated, and we would therefore expect that the relative decrease in morning transpiration due to dew would be even larger if leaf angle dynamics were taken into account.

In conclusion, our results show that dew deposition can have a large impact on transpiration suppression. In particular, we find that transpiration suppression effects vary with leaf size, with larger leaves

experiencing an enhanced impact due to the increased leaf wetness duration. In addition, CO_2 assimilation is negatively impacted by the presence of dew, because of the decrease in leaf temperature associated with it. However, we found that at high humidity and low wind speeds, large dew-wetted leaves can experience both a decrease in transpiration and an increase in assimilation, leading to an increase water use efficiency. Here we represent dew deposition as a film of water, and while we recognize that this model has its limitations, we expect that a more detailed representation of dew droplets as half-spheres would further increase transpiration suppression. This work is only the first step towards understanding the impact of water deposition on leaves. Future work should strive to tease out the relative importance of the effects of temperature, radiation, and stomata clogging on both transpiration and assimilation. In particular, understanding the mechanistic pathways of these interactions is critical to incorporate the effects of dew deposition into ecosystem-scale models.

Acknowledgments

Appendix A. Supplementary data

Supplementary data associated with this article can be found, in the online version, at https://doi.org/10.1016/j.agrformet.2018.05.015.

References

Abtew, W., Melesse, A., 2012. Evaporation and Evapotranspiration. Springer Science & Business Media, Dordrecht.

Agam, N., Berliner, P.R., 2006. Dew formation and water vapor adsorption in semi-arid environments – a review. J. Arid Environ. 65 (4), 572–590.

Alvarado-Barrientos, M.S., Holwerda, F., Asbjornsen, H., Dawson, T.E., Bruijnzeel, L.A., 2014. Suppression of transpiration due to cloud immersion in a seasonally dry Mexican weeping pine plantation. Agric. Forest Meteorol. 186, 12–25.

Andrade, J.L., 2003. Dew deposition on epiphytic bromeliad leaves: an important event in a Mexican tropical dry deciduous forest. J. Trop. Ecol. 19 (5), 479–488.

Aparecido, L.M.T., Miller, G.R., Cahill, A.T., Moore, G.W., 2017. Leaf surface traits and water storage retention affect photosynthetic responses to leaf surface wetness among wet tropical forest and semiarid savanna plants. Tree Physiol. 37 (10), 1285–1300.

Barradas, V.L., Glez-Medellín, M.G., 1999. Dew and its effect on two heliophile understorey species of a tropical dry deciduous forest in Mexico. Int. J. Biometeorol. 43 (1), 1–7.

Berkelhammer, M., Hu, J., Bailey, A., Noone, D.C., Still, C.J., Barnard, H., Gochis, D., Hsiao, G.S., Rahn, T., Turnipseed, A., 2013. The nocturnal water cycle in an open-canopy forest. J. Geophys. Res.: Atmosp. 118 (1), 10225.

Beysens, D., 1995. The formation of dew. Atmosp. Res. 39 (1), 215–237.

Beysens, D., 2005. Dew nucleation and growth. Comptes Rendus Phys. 7 (9), 1082–1100.

Beysens, D., 2016. Estimating dew yield worldwide from a few meteo data. Atmosp. Res. 167 (C), 146–155.

Beysens, D., Steyer, A., Guenoun, P., Fritter, D., Knobler, C.M., 2006. How does dew form? Phase Trans. 31 (1–4), 219–246.

Bregaglio, S., Donatelli, M., Confalonieri, R., Acutis, M., Orlandini, S., 2010. Multi metric evaluation of leaf wetness models for large-area application of plant disease models. Agric. Forest Meteorol. 151 (9), 1163–1172.

Brodribb, T., Holbrook, N., 2003. Stomatal closure during leaf dehydration, correlation with other leaf physiological traits. Plant Physiol. 132 (4), 2166–2173.

Buckley, T.N., Martorell, S., Diaz-Espejo, A., Tomas, M., Medrano, H., 2014. Is stomatal conductance optimized over both time and space in plant crowns? A field test in grapevine (*Vitis vinifera*). Plant Cell Environ. 37 (12), 2707–2721.

Campbell, G.S., Norman, J.M., 1998. An Introduction to Environmental Biophysics. Springer New York, New York, NY.

Chu, H.-S., Chang, S.-C., Klemm, O., Lai, C.-W., Lin, Y.-Z., Wu, C.-C., Lin, J.Y., Jiang, J.Y., Chen, J., Gottgens, J.F., Hsia, Y.-J., 2012. Does canopy wetness matter? Evapotranspiration from a subtropical montane cloud forest in Taiwan. Hydrol. Process. 28 (3), 1190–1214.

Chungu, C., Gilbert, J., Townley-Smith, F., 2001. *Septoria tritici* blotch development as affected by temperature, duration of leaf wetness, inoculum concentration, and host. Plant Dis. 85 (4), 430–435.

Clus, O., Ortega, P., Muselli, M., Milimouk, I., Beysens, D., 2008. Study of dew water collection in humid tropical islands. J. Hydrol. 361 (1), 159–171.

Cobos, D.R., 2013. Predicting the Amount of Water on the Surface of the LWS Dielectric Leaf Wetness Sensor. Decagon Devices, Inc. Application Note 509-332-5600.

Cook, B.I., Smerdon, J.E., Seager, R., Coats, S., 2014. Global warming and 21st century drying. Climate Dyn. 43 (9–10), 2607–2627.

Dalla Marta, A., Magarey, R.D., Martinelli, L., Orlandini, S., 2007. Leaf wetness duration in sunflower (*Helianthus annuus*): analysis of observations, measurements and simulations. Eur. J. Agron. 26 (3), 310–316.

Dalla Marta, A., Magarey, R.D., Orlandini, S., 2005. Modelling leaf wetness duration and downy mildew simulation on grapevine in Italy. Agric. Forest Meteorol. 132 (1–2), 84–95.

de Jeu, R.A.M., Holmes, T.R.H., Owe, M., 2005. Determination of the effect of dew on passive microwave observations from space. Rem. Sens. Agric. 5976, 51–59.

Dewar, R., Mauranen, A., M“akel”a, A., H“oltt”a, T., Medlyn, B., Vesala, T., 2017. New insights into the covariation of stomatal, mesophyll and hydraulic conductances from optimization models incorporating nonstomatal limitations to photosynthesis. New Phytol. 217 (October (2)), 571–585.

Dingman, S.L., 2002. Physical Hydrology, 2nd ed. Waveland Press, Inc.

Ehleringer, J.R., Comstock, J., 1987. Leaf absorptance and leaf angle: mechanisms for stress avoidance. In: Tenhunen, J.D., Catarino, F.M., Lange, O.L., Oechel, W.C. (Eds.), Plant Response to Stress: Functional Analysis in Mediterranean Ecosystems. Springer Berlin Heidelberg, Berlin, Heidelberg, pp. 55–76. http://dx.doi.org/10.1007/978-3-642-70868-8_3.

Evans, K.J., Nyquist, W.E., Latin, R.X., 1992. A model based on temperature and leaf wetness duration for establishment of alternaria leaf-blight of muskmelon. Phytopathology 82 (8), 890–895.

Fisher, J.B., Melton, F., Middleton, E., Hain, C., Anderson, M., Allen, R., McCabe, M.F., Hook, S., Baldocchi, D., Townsend, P.A., Kilic, A., Tu, K., Miralles, D.D., Perret, J., Lagouarde, J.-P., Waliser, D., Purdy, A.J., French, A., Schimel, D., Famiglietti, J.S., Stephens, G., Wood, E.F., 2017. The future of evapotranspiration: global requirements for ecosystem functioning, carbon and climate feedbacks, agricultural management, and water resources. Water Resour. Res. 53 (4), 2618–2626.

Frolking, S., Milliman, T., Palace, M., Wisser, D., Lammers, R., Fahnestock, M., 2011. Tropical forest backscatter anomaly evident in SeaWinds scatterometer morning overpass data during 2005 drought in Amazonia. Rem. Sens. Environ. 115 (3), 897–907.

Gao, L., McCarthy, T.J., 2006. Contact angle hysteresis explained. Langmuir 22 (14), 6234–6237.

Gates, D., 1980. Biophysical Ecology. Springer-Verlag New York.

Gauslaa, Y., 2014. Rain, dew, and humid air as drivers of morphology, function and spatial distribution in epiphytic lichens. Lichenologist 46 (01), 1–16.

Gerlein-Safdi, C., Gauthier, P.P.G., Caylor, K.K., 2018. Dew-induced transpiration suppression impacts the water and isotope balances of *Colocasia* leaves. Oecologia.

Gil, R., Bojaca, C.R., Schrevens, E., 2011. Suitability evaluation of four methods to estimate leaf wetness duration in a greenhouse rose crop. Acta Horticult. 797–804.

Givnish, T.J., 1987. Comparative studies of leaf form: assessing the relative roles of selective pressures and phylogenetic constraints. New Phytol. 106 (S1), 131–160.

Goldsmith, G.R., Bentley, L.P., Shenkin, A., Salinas, N., Blonder, B., Martin, R.E., Castro-Ccossco, M., Chambi-Porroa, P., Diaz, S., Enquist, B.J., Asner, G.P., Malhi, Y., 2016. Variation in leaf wettability traits along a tropical montane elevation gradient. New Phytol. 214 (3), 989–1001.

Gotsch, S.G., Nadkarni, N., Darby, A., Glunk, A., Mackenzie, D., Davidson, K., Dawson, T.E., 2015. Life in the treetops: ecophysiological strategies of canopy epiphytes in a tropical montane cloud forest. Ecol. Monogr. 85 (3), 393–412.

Guevara-Escobar, A., González-Sosa, E., Véliz-Chávez, C., Ventura-Ramos, E., Ramos-Salinas, M., 2007. Rainfall interception and distribution patterns of gross precipitation around an isolated *Ficus benjamina* tree in an urban area. J. Hydrol. 333 (2–4), 532–541.

Hamilton, M.P., Dawson, T.E., Thompson, S.E., 2011. The very large ecological array. AGU Fall Meeting Abstracts, Abstract B14A-08.

Hill, A.J., Dawson, T.E., Shelef, O., Rachmilevitch, S., 2015. The role of dew in Negev Desert plants. Oecologia 178 (2), 317–327.

Holder, C.D., 2012a. Effects of leaf hydrophobicity and water droplet retention on canopy storage capacity. Ecohydrology 6 (3), 483–490.

Holder, C.D., 2012b. The relationship between leaf hydrophobicity, water droplet retention, and leaf angle of common species in a semi-arid region of the western United States. Agric. Forest Meteorol. 152, 11–16.

Holloway, P.J., 1994. chap. Plant cuticles: physiochemical characteristics and biosynthesis. In: Percy, K., Cape, C.N., Jagels, R., Simpson, C.J. (Eds.), Air Pollutants and the Leaf Cuticle. Springer, Heidelberg, Germany.

Incropera, F.P., DeWitt, D.P., Bergman, T.L., Lavine, A.S., 2007. Fundamentals of Heat and Mass Transfer, 6th ed. John Wiley, Hoboken, NJ.

Jacobs, A.F.G., Heusinkveld, B.G., Berkowicz, S.M., 2002. A simple model for potential dewfall in an arid region. Atmosp. Res. 64 (1), 285–295.

Jacobs, A.F.G., Heusinkveld, B.G., Wichink Kruit, R.J., Berkowicz, S.M., 2006. Contribution of dew to the water budget of a grassland area in the Netherlands. Water Resour. Res. 42 (3).

Janssen, L.H.J.M., Römer, F.G., 1991. The frequency and duration of dew occurrence over a year: model results compared with measurements. Tellus B 43 (5), 408.

Jordan, D.N., Smith, W.K., 1994. Energy balance analysis of nighttime leaf temperatures and frost formation in a subalpine environment. Agric. Forest Meteorol. 71 (3), 359–372.

Kabela, E.D., Hornbuckle, B.K., Cosh, M.H., Anderson, M.C., Gleason, M.L., 2009. Dew frequency, duration, amount, and distribution in corn and soybean during SMEX05. Agric. Forest Meteorol. 149 (1), 11–24.

Katata, G., Kajino, M., Hiraki, T., Aikawa, M., 2011. A method for simple and accurate estimation of fog deposition in a mountain forest using a meteorological model. J. Geophys. Res. 116 (20), D20102.

Kim, K.S., Taylor, S.E., Gleason, M.L., Nutter Jr., F.W., Coop, L.B., Pfender, W.F., Seem, R.C., Sentelhas, P.C., Gillespie, T.J., Marta, A.D., Orlandini, S., Dalla Marta, A., 2010. Spatial portability of numerical models of leaf wetness duration based on empirical approaches. Agric. Forest Meteorol. 150 (7–8), 871–880.

King, D.A., 1997. The functional significance of leaf angle in Eucalyptus. Aust. J. Bot. 45 (4), 619–639.

Konrad, W., Burkhardt, J., Ebner, M., Roth-Nebelsick, A., 2014. Leaf pubescence as a possibility to increase water use efficiency by promoting condensation. Ecohydrology 8 (3), 480–492.

Kooperman, G.J., Chen, Y., Hoffman, F.M., Koven, C.D., Lindsay, K., Pritchard, M.S., Swann, A.L.S., Randerson, J.T., 2018. Forest response to rising CO_2 drives zonally asymmetric rainfall change over tropical land. Nat. Climate Change 8 (April (5)), 434–440.

Kustas, W.P., Rango, A., Uijlenhoet, R., 1994. A simple energy budget algorithm for the snowmelt runoff model. Water Resour. Res. 30 (May (5)), 1515–1527.

Lakatos, M., Obregón, A., B”udel, B., Bendix, J., 2012. Midday dew – an overlooked factor enhancing photosynthetic activity of corticolous epiphytes in a wet tropical rain forest. New Phytol. 194 (1), 245–253.

Leach, R.N., Stevens, F., Langford, S.C., Dickinson, J.T., 2006. Dropwise condensation: experiments and simulations of nucleation and growth of water drops in a cooling system. Langmuir 22 (21), 8864–8872.

Letts, M.G., Mulligan, M., 2005. The impact of light quality and leaf wetness on photosynthesis in north-west Andean tropical montane cloud forest. J. Trop. Ecol. 21 (05), 549–557.

Leuning, R., 1988. Leaf temperatures during radiation frost Part II. A steady state theory. Agric. Forest Meteorol. 42 (2), 135–155.

Li, S., Zhang, Y.-J., Sack, L., Scoffoni, C., Ishida, A., Chen, Y.-J., Cao, K.-F., 2013. The heterogeneity and spatial patterning of structure and physiology across the leaf surface in giant leaves of *Alocasia macrorrhiza*. PLoS ONE 8 (6), e66016.

Lloyd, J., Farquhar, G.D., 1994. ^{13}C discrimination during CO_2 assimilation by the terrestrial biosphere. Oecologia 99 (3–4), 201–215.

Madeira, A.C., Kim, K.S., Taylor, S.E., Gleason, M.L., 2002. A simple cloud-based energy balance model to estimate dew. Agric. Forest Meteorol. 111 (1), 55–63.

Maestre-Valero, J.F., Ragab, R., Martínez-Alvarez, V., Baille, A., 2012. Estimation of dew yield from radiative condensers by means of an energy balance model. J. Hydrol. 460–461 (C), 103–109.

Malhi, Y., Wright, J., 2004. Spatial patterns and recent trends in the climate of tropical rainforest regions. Philos. Trans. R. Soc. B: Biol. Sci. 359 (1443), 311–329.

McLaughlin, B.C., Ackerly, D.D., Klos, P.Z., Natali, J., Dawson, T.E., Thompson, S.E., 2017. Hydrologic refugia, plants, and climate change. Global Change Biol. 66, 107–121.

Medlyn, B.E., Duursma, R.A., Eamus, D., Ellsworth, D.S., Prentice, I.C., Barton, C.V.M., Crous, K.Y., De Angelis, P., Freeman, M., Wingate, L., 2011. Reconciling the optimal and empirical approaches to modelling stomatal conductance. Global Change Biol. 17 (6), 2134–2144.

Monteith, J.L., 1957. Dew. Q. J. R. Meteorol. Soc. 83, 322–341.

Monteith, J.L., 1963. In: Rutter, A.J., Whitehead, F.H. (Eds.), The Water Relations of Plants. Blackwell Scientific, New York, pp. 37–56.

Moreira, M., Sternberg, L., Martinelli, L., Victoria, R., Barbosa, E., Bonates, L., Nepstad,

D., 1997. Contribution of transpiration to forest ambient vapour based on isotopic measurements. Global Change Biol. 3 (5), 439–450.

Neinhuis, C., Barthlott, W., 1997. Characterization and distribution of water-repellent, self-cleaning plant surfaces. Ann. Bot. 79 (6), 667–677.

Nepstad, D.C., Stickler, C.M., Soares-Filho, B., Merry, F., 2008. Interactions among Amazon land use, forests and climate: prospects for a near-term forest tipping point. Philos. Trans. R. Soc. B: Biol. Sci. 363 (1498), 1737–1746.

Nikolayev, V.S., Beysens, D., Gioda, A., Milimouka, I., Katiushin, E., Morel, J.P., 1996. Water recovery from dew. J. Hydrol. 182 (1), 19–35.

Pan, Y., Wang, X., 2014. Effects of shrub species and microhabitats on dew formation in a revegetationstabilized desert ecosystem in Shapotou, northern China. J. Arid Land 6 (4), 389–399.

Pieruschka, R., Huber, G., Berry, J.A., 2010. Control of transpiration by radiation. Proc. Natl. Acad. Sci. U. S. A. 107 (30), 13372–13377.

Pinter Jr., P.J., 1986. Effect of dew on canopy reflectance and temperature. Rem. Sens. Environ. 19 (2).

Posada, J.M., Siev“anen, R., Messier, C., Perttunen, J., Nikinmaa, E., Lechowicz, M.J., 2012. Contributions of leaf photosynthetic capacity, leaf angle and self-shading to the maximization of net photosynthesis in Acer saccharum: a modelling assessment. Ann. Bot. 110 (3), 731–741.

Proctor, M.C.F., 2012. Dew, where and when? 'There are more things in heaven and earth, Horatio, than are dreamt of in your philosophy'. New Phytol. 194 (1), 10–11.

Ray, D.K., Nair, U.S., Lawton, R.O., Welch, R.M., Pielke, R.A., 2006. Impact of land use on Costa Rican tropical montane cloud forests: sensitivity of orographic cloud formation to deforestation in the plains. J. Geophys. Res.: Atmosp. 111 (D), D02108.

Richards, K., 2009. Adaptation of a leaf wetness model to estimate dewfall amount on a roof surface. Agric. Forest Meteorol. 149 (8), 1377–1383.

Rodriguez-Dominguez, C.M., Buckley, T.N., Egea, G., de Cires, A., Hernandez-Santana, V., Martorell, S., Diaz-Espejo, A., 2016. Most stomatal closure in woody species under moderate drought can be explained by stomatal responses to leaf turgor. Plant Cell Environ. 39 (9), 2014–2026.

Rodriguez-Iturbe, I., Porporato, A., 2004. Ecohydrology of Water-Controlled Ecosystems. Cambridge University Press, New York.

Rosenzweig, C., Abramopoulos, F., 1997. Land-surface model development for the GISS GCM. J. Climate 10 (8), 2040–2054.

Rossi, V., Caffi, T., Giosu, S., Bugiani, R., 2008. A mechanistic model simulating primary infections of downy mildew in grapevine. Ecol. Modell. 212 (3–4), 480–491.

Schmitz, H.F., Grant, R.H., 2009. Precipitation and dew in a soybean canopy: spatial variations in leaf wetness and implications for *Phakopsora pachyrhizi* infection. Agric. Forest Meteorol. 149 (10), 1621–1627.

Schuepp, P.H., 1993. Leaf Boundary Layers: Tansley Review no. 59 (Vol. 125). New Phytologist.

Schymanski, S.J., Or, D., 2016. Wind increases leaf water use efficiency. Plant Cell Environ. 39 (7), 1448–1459.

Schymanski, S.J., Or, D., Zwieniecki, M., 2013. Stomatal control and leaf thermal and hydraulic capacitances under rapid environmental fluctuations. PLoS ONE 8 (1), e54231.

Scoffoni, C., Rawls, M., McKown, A., Cochard, H., Sack, L., 2011. Decline of leaf hydraulic conductance with dehydration: relationship to leaf size and venation architecture. Plant Physiol. 156 (2), 832–843.

Sellers, B., 2003. Diurnal fluctuations and leaf angle reduce glufosinate efficacy. Weed Technol. 17 (2), 302–306.

Sentelhas, P.C., Dalla Marta, A., Orlandini, S., Santos, E.A., Gillespie, T.J., Gleason, M.L., 2008. Suitability of relative humidity as an estimator of leaf wetness duration. Agric. Forest Meteorol. 148 (3), 392–400.

Tanaka, K., 2002. Multi-layer model of CO_2 exchange in a plant community coupled with the water budget of leaf surfaces. Ecol. Modell. 147 (1), 85–104.

Tenhunen, J.D., Lange, O.L., Braun, M., 1981. Midday stomatal closure in Mediterranean type sclerophylls under simulated habitat conditions in an environmental chamber – II. Effect of the complex of leaf temperature and air humidity on gas exchange of *Arbutus unedo* and *Quercus ilex*. Oecologia 50 (August (1)), 5–11.

Tolk, J.A., Howell, T.A., Steiner, J.L., Krieg, D.R., Schneider, A.D., 1995. Role of transpiration suppression by evaporation of intercepted water in improving irrigation efficiency. Irrig. Sci. 16 (2), 89–95.

Tomaszkiewicz, M., Najm, M.A., Beysens, D., Alameddine, I., Zeid, E.B., El-Fadel, M., 2016. Projected climate change impacts upon dew yield in the Mediterranean basin. Sci. Total Environ. 566–567, 1339–1348.

Uclés, O., Villagarcía, L., Moro, M.J., Canton, Y., Domingo, F., 2013. Role of dewfall in the water balance of a semiarid coastal steppe ecosystem. Hydrol. Process. 28 (4), 2271–2280.

Vico, G., Manzoni, S., Palmroth, S., Weih, M., Katul, G., 2013, December. A perspective on optimal leaf stomatal conductance under CO_2 and light co-limitations. Agric. Forest Meteorol. 182–183, 191–199.

Vogel, S., 2012. The Life of a Leaf. The University of Chicago Press.

Vuollekoski, H., Vogt, M., Sinclair, V.A., Duplissy, J., J”arvinen, H., Kyrö, E.-M., Makkonen, R., Petäjä, T., Prisle1, N.L., Räisänen, P., Sipilä, M., Ylhäisi, J., Kulmala, M., 2015. Estimates of global dew collection potential on artificial surfaces. Hydrol. Earth Syst. Sci. 19 (1), 601–613.

Wilson, T.B., Bland, W.L., Norman, J.M., 1999. Measurement and simulation of dew accumulation and drying in a potato canopy. Agric. Forest Meteorol. 93 (2), 111–119.

Wolf, A., Anderegg, W.R.L., Pacala, S.W., 2016. Optimal stomatal behavior with competition for water and risk of hydraulic impairment. PNAS 113 (46), E7222–E7230.

Xu, Y., Yan, B., Tang, J., 2015. The effect of climate change on variations in dew amount in a paddy ecosystem of the Sanjiang Plain, China. Adv. Meteorol. 2015 (2), 1–9.

Yamaguchi, T., Noguchi, I., Watanabe, Y., Katata, G., Sato, H., Hara, H., 2013. Aerosol deposition and behavior on leaves in cool-temperate deciduous forests. Part 2: characteristics of fog water chemistry and fog deposition in Northern Japan. Asian J. Atmosp. Environ. 7 (1), 8–16.

Yang, X.-D., Lv, G.-H., Ali, A., Ran, Q.-Y., Gong, X.-W., Wang, F., Liu, Z.-D., Qin, L., Liu, W.-G., 2017. Experimental variations in functional and demographic traits of *Lappula semiglabra* among dew amount treatments in an arid region. Ecohydrology 10 (6), e1858.

Yates, D.J., Hutley, L.B., 1995. Foliar uptake of water by wet leaves of *Sloanea woollsii*, an Australian subtropical rainforest tree. Aust. J. Bot. 43 (2), 157–167.

Zangvil, A., 1996. Six years of dew observations in the Negev Desert, Israel. J. Arid Environ. 32 (4), 361–371.

Zimmermann, B., Zimmermann, A., Scheckenbach, H.L., Schmid, T., Hall, J.S., van Breugel, M., 2013. Changes in rainfall interception along a secondary forest succession gradient in lowland Panama. Hydrol. Earth Syst. Sci. 17 (11), 4659–4670.